

Journal of Quaternary Science



Check for updates

The preservation of storm events in the geologic record of New Jersey, USA

KRISTEN M. JOYSE, ^{1,2}* D JENNIFER S. WALKER, ³ LINDA GODFREY, ² MARGARET A. CHRISTIE, ⁴ TIMOTHY A. SHAW, ¹ D. REIDE CORBETT, ⁵ ROBERT E. KOPP^{2,6} and BENJAMIN P. HORTON^{1,7}

¹Earth Observatory of Singapore, Nanyang Technological University, Singapore

Received 2 May 2023; Revised 21 February 2024; Accepted 28 April 2024

ABSTRACT: Geologic reconstructions of overwash events can extend storm records beyond the brief instrumental record. However, the return periods of storms calculated from geologic records alone may underestimate the frequency of events given the preservation bias of geologic records. Here, we compare a geologic reconstruction of storm activity from a salt marsh in New Jersey to two neighboring instrumental records at the Sandy Hook and Battery tide gauges. Eight overwash deposits were identified within the marsh's stratigraphy by their fan-shaped morphology and coarser mean grain size $(3.6 \pm 0.7 \,\phi)$ compared to autochthonous sediments they were embedded in $(5.6 \pm 0.8 \,\phi)$. We used an age–depth model based on modern chronohorizons and three radiocarbon dates to provide age constraints for the overwash deposits. Seven of the overwash deposits were attributed to historical storms, including the youngest overwash deposit from Hurricane Sandy in 2012. The four youngest overwash deposits overlap with instrumental records. In contrast, the Sandy Hook and Battery tide gauges recorded eight and 11 extreme water levels above the 10% annual expected probability (AEP) of exceedance level, respectively, between 1932/1920 and the present. The geologic record in northern New Jersey, therefore, has a 36–50% preservation potential of capturing extreme water levels above the 10% AEP level. © 2024 The Authors. *Journal of Quaternary Science* Published by John Wiley & Sons Ltd.

KEYWORDS: extreme water levels; overwash deposit; salt marsh; storm surge

Introduction

Tropical cyclones (TCs) and extratropical cyclones (ETCs) are climatologically complex systems that can produce extensive damage to coastal communities and infrastructure from storm surges (e.g. Mendelsohn et al., 2012, Ranson et al., 2014). The densely populated mid-Atlantic US is regularly impacted by landfalling TCs and ETCs and attendant storm surges (e.g. Brandon et al., 2014, Rappaport, 2014), but tide gauge records are too short to support robust conclusions regarding how natural and anthropogenic climate forcings control the frequency of TCs and ETCs (Muller et al., 2017, Seneviratne et al., 2021).

Geologic reconstructions of overwash events from TC- and ETC-induced storm surges can extend the record of land-falling TC and ETC activity beyond the short instrumental era (e.g. Liu & Fearn 1993, 2000; Donnelly et al., 2001b, 2004). Overwash events occur when a high-energy storm surge erodes and transports sediment from foreshore environments inland (e.g. Liu, 2004, Donnelly & Webb 2004, Donnelly et al., 2001a). As energy from surge waters dissipates, allochthonous sediments are deposited from suspension into low-energy environments such as salt marshes (Liu, 2004). If an overwash deposit is preserved and incorporated into the geologic record, it can be identified as a sedimentologically distinct fan-shaped layer with a characteristi-

cally larger grain size and lower organic content compared to typical low-energy sediments (e.g. Donnelly et al., 2001b, 2004; Scileppi & Donnelly 2007; Castagno et al., 2021). Overwash deposits can be further identified by verifying the foreshore provenance of the allochthonous sediments. This has classically been achieved through comparison of microfossil assemblages (e.g. Hippensteel & Martin, 1999, Horton & Sawai, 2010, Pilarczyk et al., 2014) and geochemical signatures (e.g. Lambert et al., 2008, Das et al., 2013) of a suspected overwash deposit with those of the surrounding low-energy sediments.

Geologic overwash deposits have been used to determine past periods of heightened TC activity and to estimate local return periods for extreme water level events (e.g. Kiage et al., 2011, Lin et al., 2014, Donnelly et al., 2015). However, not all storm-generated overwash deposits are incorporated undisturbed into the geologic record, and not all storms have the necessary intensity, track and timing to produce an overwash event in a given location (Liu 2004, Hippensteel, 2011, Muller et al., 2017, Wallace et al., 2021). To accurately interpret periods of heightened storm activity or calculate return periods of extreme water level events from geologic records of overwash deposits, it is vital to determine the preservation bias of the geologic record (Hippensteel, 2011). Estimates of return periods from geologic deposits may underestimate the long-term return periods of extreme coastal water level events if they do not account for the number of overwash deposits missing from the geologic record (Hippensteel, 2011).

*Correspondence: Kristen M. Joyse, as above. E-mail: kristen.joyse@alluvium.com.au

²Department of Earth and Planetary Sciences, Rutgers University, Piscataway, NJ, USA

³Department of Environmental Science, Rowan University, Glassboro, NJ, USA

⁴Department of Environmental Studies, McDaniel College, Westminster, MD, USA

⁵Department of Coastal Studies, East Carolina University, Wanchese, NC, USA

⁶Rutgers Climate and Energy Institute, Rutgers University, New Brunswick, NJ, USA

⁷Asian School of the Environment, Nanyang Technological University, Singapore

The widespread creation and comparison of geologic overwash records to local instrumental records from tide gauges is necessary to resolve the question of geologic preservation potentials of storm overwash events (Wallace et al., 2021).

This study generates a new geologic record of overwash events from a salt marsh in Cheesequake State Park in northern New Jersey, USA (Figure 1), to determine the preservation potential of the regional geologic record in capturing overwash events. This region was heavily impacted by Hurricane Sandy in 2012, which made landfall as a post-tropical cyclone in southern New Jersey (Blake et al., 2013). The overwash deposit produced by Hurricane Sandy provided a modern analogue to identify older overwash deposits. We use grain size, organic content, organic stable carbon isotopes and foraminiferal abundances to identify overwash deposits from the salt marsh at Cheesequake State Park (Joyse et al. 2023). The geologic record is dated using modern chronohorizons, including heavy metal pollution markers, ¹³⁷Cs and pollen abundances, in conjunction with radiocarbon dating. We compare our geologic record of overwash deposits with extreme water level events (above the 10% annual expected probability of exceedance level) recorded by the nearby Sandy Hook, New Jersey (Figure 2), and the Battery, New York, tide gauges (two of the longest-recording tide gauges in the USA) to determine the preservation bias of the geologic record in northern New Jersey. Understanding the preservation of overwash deposits has implications for extreme water level event return periods for northern New Jersey.

Study area

Cheesequake State Park consists of a complex system of tidal marshes, channels and creeks located along the northern coast of New Jersey within Raritan Bay (Figure 1). The salt marshes at Cheesequake accumulated during the late Holocene in response to accommodation space created by glacio-isostatic adjustment (GIA) subsidence causing relative sea-level rise (RSLR) in the region (e.g. Shaw & Ceman, 1999; Walker et al., 2021, 2022). A geologic reconstruction of RSLR from Cheesequake State Park shows relative sea level rose at an average rate of 1.5 ± 0.2 mm a^{-1} from 1000 to 2000 CE (Figure 2) (Walker et al., 2021), while modern rates of RSLR emerged from background Common Era variability in the late nineteenth century (Walker et al., 2022). Instrumental rates of RSLR from the Sandy Hook tide gauge, located ~20 km to the east of Cheesequake State Park, are $4.15 \pm 0.20 \text{ mm a}^{-1}$ from 1932 to 2020 cE (NOAA, 2021), which is higher than global mean sea-level rise $(1.6 \pm 0.4 \text{ mm a}^{-1} 1900)$ to 2015 CE) (Dangendorf et al., 2019) due to a combination of GIA, sediment compaction and groundwater withdrawal at Sandy Hook (Johnson et al. 2018).

The understanding of past storm activity at Cheesequake State Park is complicated by urban land development and the presence

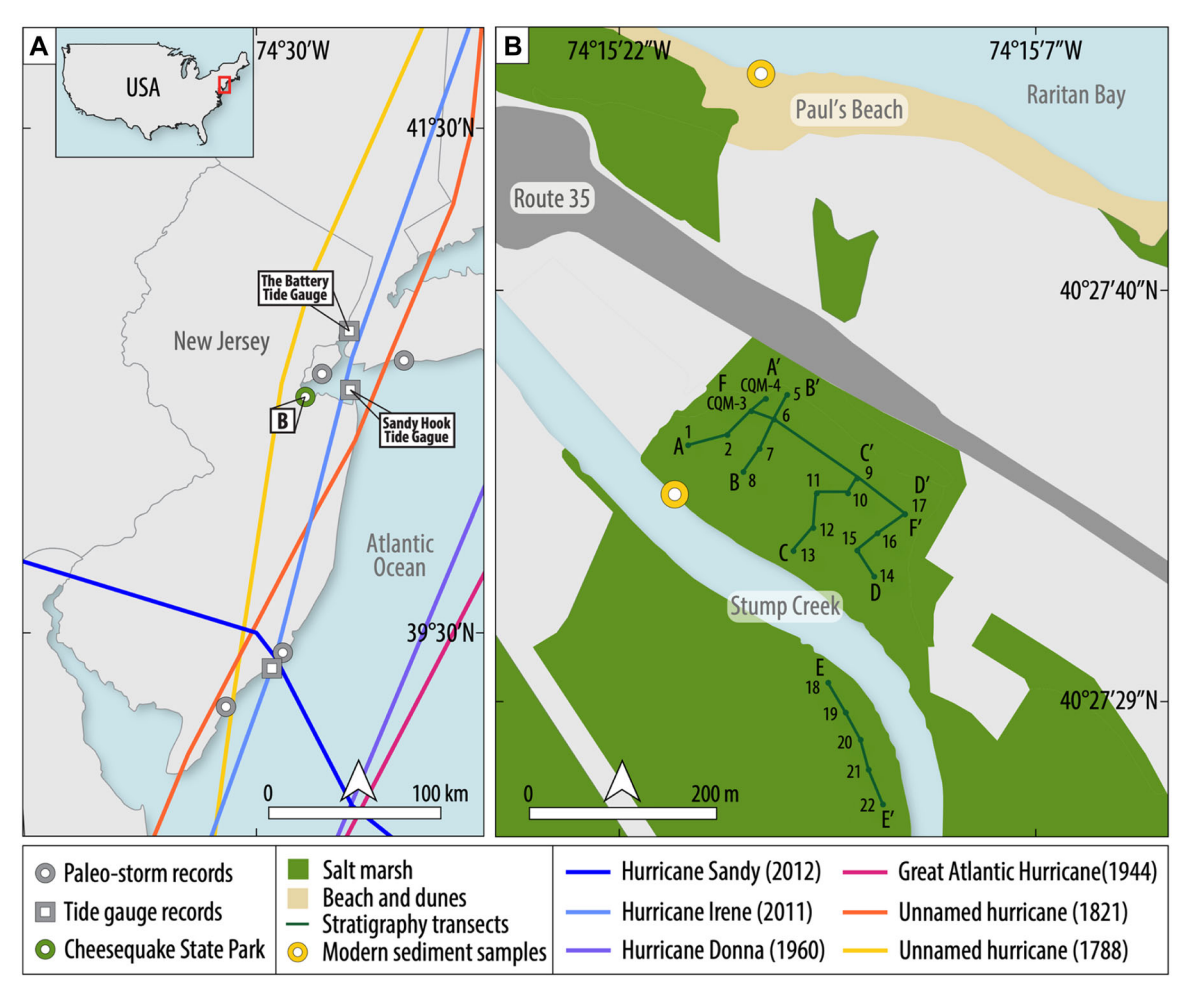


Figure 1. (A) Regional map of New Jersey with lines depicting the paths of major hurricanes that were registered on the Sandy Hook tide gauge or found in southern New Jersey paleo-storm studies including the paths of Hurricane Sandy (2012), Hurricane Irene (2011), Hurricane Donna (1960), the 1944 Great Atlantic Hurricane, the 1821 pre-instrumental hurricane and the 1788 pre-instrumental hurricane. Locations of the Sandy Hook, Battery and Atlantic City tide gauges are shown by gray squares, and the locations of neighboring paleo-storm records from New York (Brandon et al., 2014, Scileppi & Donnelly, 2007) and southern New Jersey (Donnelly et al., 2004) are shown by gray circles. (B) Site map of the marsh in Cheesequake State Park with coring transects and locations of modern sediment samples shown by yellow circles. [Color figure can be viewed at wileyonlinelibrary.com]

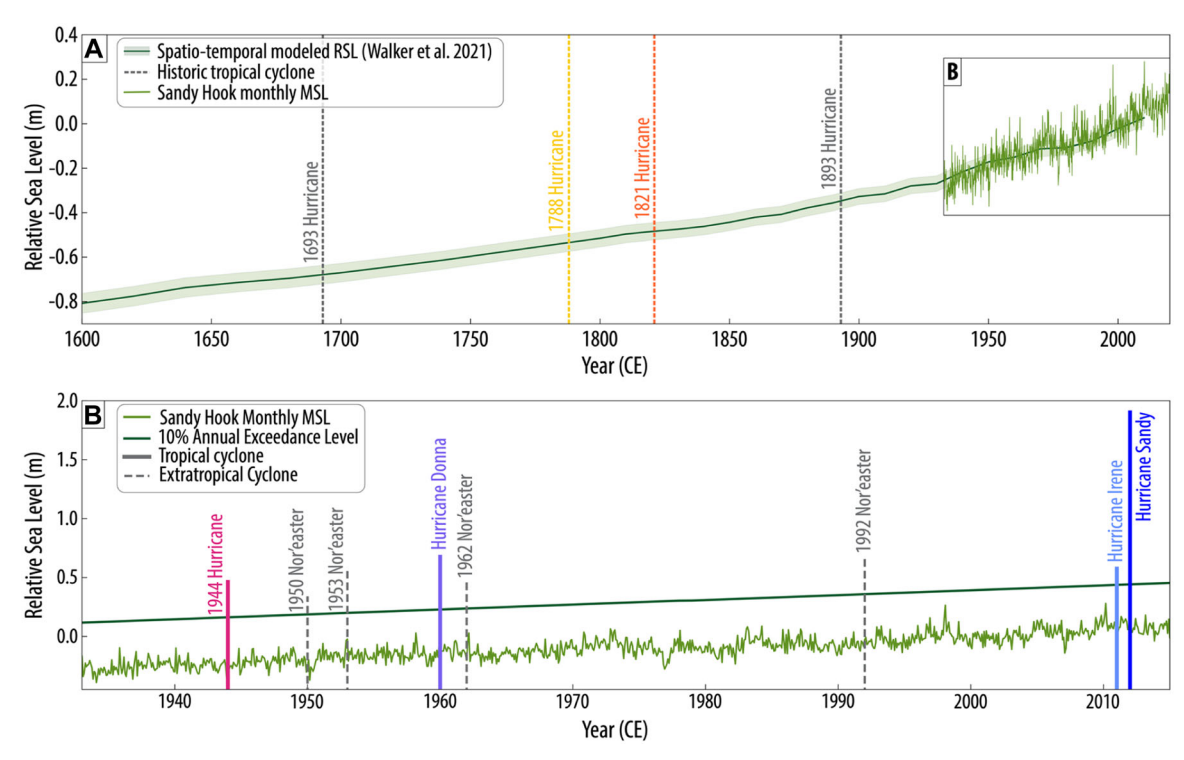


Figure 2. (A) Spatio-temporal model reconstruction of relative sea level from Cheesequake State Park with 1σ uncertainty (Walker et al., 2021). Monthly mean sea level from the Sandy Hook tide gauge is overlayed, and the timings of pre-industrial storms captured in regional paleo-storm records are marked by dashed lines. (B) Monthly mean sea level from the Sandy Hook tide gauge and the 10% annual exceedance water level for the Sandy Hook tide gauge. Vertical lines are the heights of the eight major water level events exceeding the 10% chance annual exceedance level recorded at the Sandy Hook tide gauge from TCs and ETCs. [Color figure can be viewed at wileyonlinelibrary.com]

of both landfalling TCs and ETCs (Boldt et al., 2010, Wallace et al., 2014); however, establishing geologic records here is important given the dense populations and infrastructure investment. Our study site is at the northeastern-most point of Cheesequake State Park. The modern salt marsh is situated with Stump Creek to its southwest, commercial and residential properties to its northwest and southeast, and New Jersey State Route 35 to its northeast (Figure 1b). Historical maps show access roads were added to a section of Route 35 that is ~300 m northwest of the Cheesequake marsh between 1943 and 1954 (U.S. Geological Survey, 1943, 1954). The addition of these roads altered the path of Stump Creek where it connects to Cheesequake Creek (U.S. Geological Survey, 1943, 1954). Beyond Route 35 lie beach dunes and open waters of Raritan Bay, where storm surges erode and transport sediment from foreshore environments inland. Anthropogenic changes to the beach and dunes (i.e. groin emplacement) lying to the northeast of the Cheesequake marsh indicate there may have been changes to the sediment source of overwash deposits found within the marsh through time (U.S. Geological Survey, 1943, 1954). Possible sources of overwash sediment include the beach and dunes at Paul's Beach or Stump Creek (Figure 1).

The modern vegetation at Cheesequake marsh comprises *Sporobolus pumilus, Sporobolus alterniflorus* and *Salicornia maritima*. The border separating the marsh from Route 35 and surrounding properties is lined with *Phragmites australis*. Cheesequake Creek has a semi-diurnal, micro-tidal regime with a total range of 1.6 m (NOAA, 2021). Present (1983–2001) mean higher high water (MHHW) at the Cheesequake Creek and Sandy Hook tide gauges is 1.7 and 1.6 m, respectively (NOAA, 2021).

Storm surges in northern New Jersey

Water level data from the Sandy Hook tide gauge (Figure 1) are available from 1932 to present (NOAA, 2021). As of

December 2021, four TCs and four ETCs have impacted northern New Jersey and created storm surges in the Sandy Hook record at or exceeding the estimated 10% annual expected probability (AEP) of exceedance level (Figure 2 and Table 1) (NOAA, 2021). Water level data from the Battery tide gauge (Figure 1) are available from 1920 to present (NOAA, 2021). As of December 2021, five TCs and six ETCs have impacted New York City and created storm surges at the Battery tide gauge at or exceeding the estimated 10% AEP level (Table 1). The 10% AEP level is commonly used in government strategic plans to prepare for extreme coastal events (e.g. Kopp et al. 2019, Sweet et al., 2022). The 10% AEP level at each tide gauge changes with the position of sea level, which changes as a function of the rate of RSLR at each tide gauge (NOAA, 2021). For example, the water level that must be exceeded to produce a 10% AEP event in 1920 cE is lower than the water level that must be exceeded in 2020 cE to create a 10% AEP event.

One extreme water level that was recorded at both the Sandy Hook and Battery tide gauges originated from Hurricane Sandy, which made landfall near Brigantine, NJ, on 29 October 2012 with 70 kt maximum sustained winds and a minimum pressure of 945 mb (Blake et al., 2013). Although Hurricane Sandy weakened prior to making landfall, the immense size and slow forward motion of the storm produced extensive flooding from New Jersey through southern New England (Blake et al., 2013). The maximum water level produced by Hurricane Sandy at both the Sandy Hook and Battery tide gauges was 2.7 m above MHHW (NOAA, 2021). Eyewitness accounts from homeowners whose properties border the Cheesequake marsh and who were present during the storm indicated that Hurricane Sandy produced a substantial storm surge throughout the study area.

Table 1. Water level heights produced by storms that exceed the 10% expected annual exceedance level at the Sandy Hook and/or Battery tide gauges.

	Year	Water level (m above MHHW)		
Event		Sandy Hook Tide Gauge	Battery Tide Gauge	
Hurricane Sandy	2012	2.71	2.74	
Hurricane Irene	2011	1.38	1.36	
Nor'easter	2010	1.16	1.14	
Nor'easter	1992	1.48	1.42	
Nor'easter	1991	1.01	1.12	
Ash Wednesday Nor'easter	1962	1.27	1.18	
Hurricane Donna	1960	1.48	1.51	
Nor'easter	1953	1.36	1.36	
Nor'easter	1950	1.15	1.24	
Unnamed Hurricane	1944	1.27	0.87	
Unnamed Hurricane	1938	0.57	0.78	

Methods

Site selection and stratigraphy

Cheesequake State Park was selected because it met the following desired criteria (Donnelly & Webb, 2004, Bregy et al., 2018): (1) a low energy environment (e.g. salt marsh); (2) proximity to a coastal barrier (e.g. dune system) that delivers a sediment source for overwash deposits; and (3) inundation by Hurricane Sandy in 2012 to provide a modern analogue overwash deposit.

From 2018 to 2020, 22 cores were taken up to a depth of 5 m to describe the sediment stratigraphy across the marsh (Figure 1b). We described sediments using the Troels-Smith classification system (Troels-Smith, 1955) and measured core top elevations of transects A–D using real time kinematic (RTK) satellite navigation and referenced to North American Vertical Datum 1988 (NAVD88).

We selected core CQM-3 for detailed analyses because of the presence of multiple overwash deposits which correlated with adjacent cores (Figure 3). We used a Russian peat corer to retrieve an undisturbed stratigraphic section to a depth of 2.5 m. Sediments recovered were stored in cut PVC pipe and plastic wrap and refrigerated at 0–4 °C. Sub-samples were collected for sedimentological, geochemical and microfossil analyses at 1- to 5-cm intervals, depending on the presence of overwash deposits within the core's stratigraphy, such that samples were taken at 1-cm intervals within and around overwash deposits and at 5-cm intervals where no overwash sediments were present. Core CQM-4, adjacent to CQM-3 (Figure 3), was similarly sampled and measured via grain size analysis to ensure coarse anomalies in mean grain size were consistent across cores (Supporting Information Fig. S2).

We sampled modern surface sediments of 1-cm thickness from Paul's Beach in Old Bridge Waterfront Park and from Stump Creek (Figure 1b) for grain size and foraminifera to identify potential sources of sediment for the overwash deposits. To ensure that older overwash deposits originated from storm surge rather than terrestrial flooding events, we analyzed the catchment sizes and river gauges from neighboring Cheesequake Creek and Raritan River.

Sedimentological analyses

Samples of CQM-3 and CQM-4 and modern sediment samples from Paul's Beach and Stump Creek were prepared for grain size analysis by digesting sediments in $30\%~H_2O_2$ to remove all organic material (Donato et al., 2009). Samples were kept at 60 °C in a hot water bath to increase the speed of the digestion (Donato et al., 2009) and were triple rinsed with deionized

water upon completion. Grain size distributions were measured with a Malvern Mastersizer 3000 laser particle analyzer, and grain size statistics were calculated using the Folk and Ward (1957) method via GRADISTAT software (Blott and Pye, 2001).

Organic content was measured through loss-on-ignition (LOI) for each sample of CQM-3. First, the dry weight of each sample was determined by drying sediments at 105 °C for 24 h (Dean, 1974). The percent organic content of samples was then determined by combusting samples in a muffle furnace for 3 h at 550 °C and calculating the mass loss of each sample (Dean, 1974).

Geochemical analyses

Organic stable carbon and C/N samples from CQM-3 were digested in 10% HCl and triple rinsed with deionized water before being dried at 45 °C for 24 h. Sediments were milled to a fine powder with a mortar and pestle and weighed into tin capsules (Khan et al., 2015a, 2015b). Samples were analyzed using a GVI Isoprime continuous-flow isotope ratio mass spectrometer (CF-IRMS) at Rutgers University; blank capsules, certified isotope standards and in-house sediment standards were included in each batch of isotopic analysis.

Foraminifera analyses

Each foraminifera sample from CQM-3 and the modern surface containing 5 cm 3 of sediment was washed, sieved for specimens sized between 500 and 63 μ m, and wet split in eight equal aliquots (Horton and Edwards, 2006). Foraminifera in one-eighth of each sample were identified and counted using a binocular microscope. Taxonomic classifications followed published literature for New Jersey salt marshes (e.g. Kemp et al., 2012, Walker et al., 2020).

Chronology

Modern geochemical chronohorizons (bulk Pb, Pb isotopic ratios, ¹³⁷Cs) were used in conjunction with radiocarbon dating to determine the age of deposition of overwash events in CQM-3. Three pollen chronohorizons were also assigned to depths in CQM-3 following regional pollen analyses that show clear changes in pollen assemblages coinciding with land-use changes following European settlement in the eastern US (Christie et al., 2021). Additional information regarding the sampling and analysis of modern chronohorizons can be found in Appendix 1.

The timing of Hurricane Sandy's landfall, modern chronohorizons and radiocarbon ages were input into an accumula-

1.0 Downloaded from https://onlinelibrary.vileje.com/doi/10.1002/qs.3622 by Rutgers University Libraries, Wiley Online Library on [29/05/2024]. See the Terms and Conditions (https://onlinelibrary.vileje.com/terms-and-conditions) on Wiley Online Library for rules of use; OA articles are governed by the applicable Creative Commons Licenses

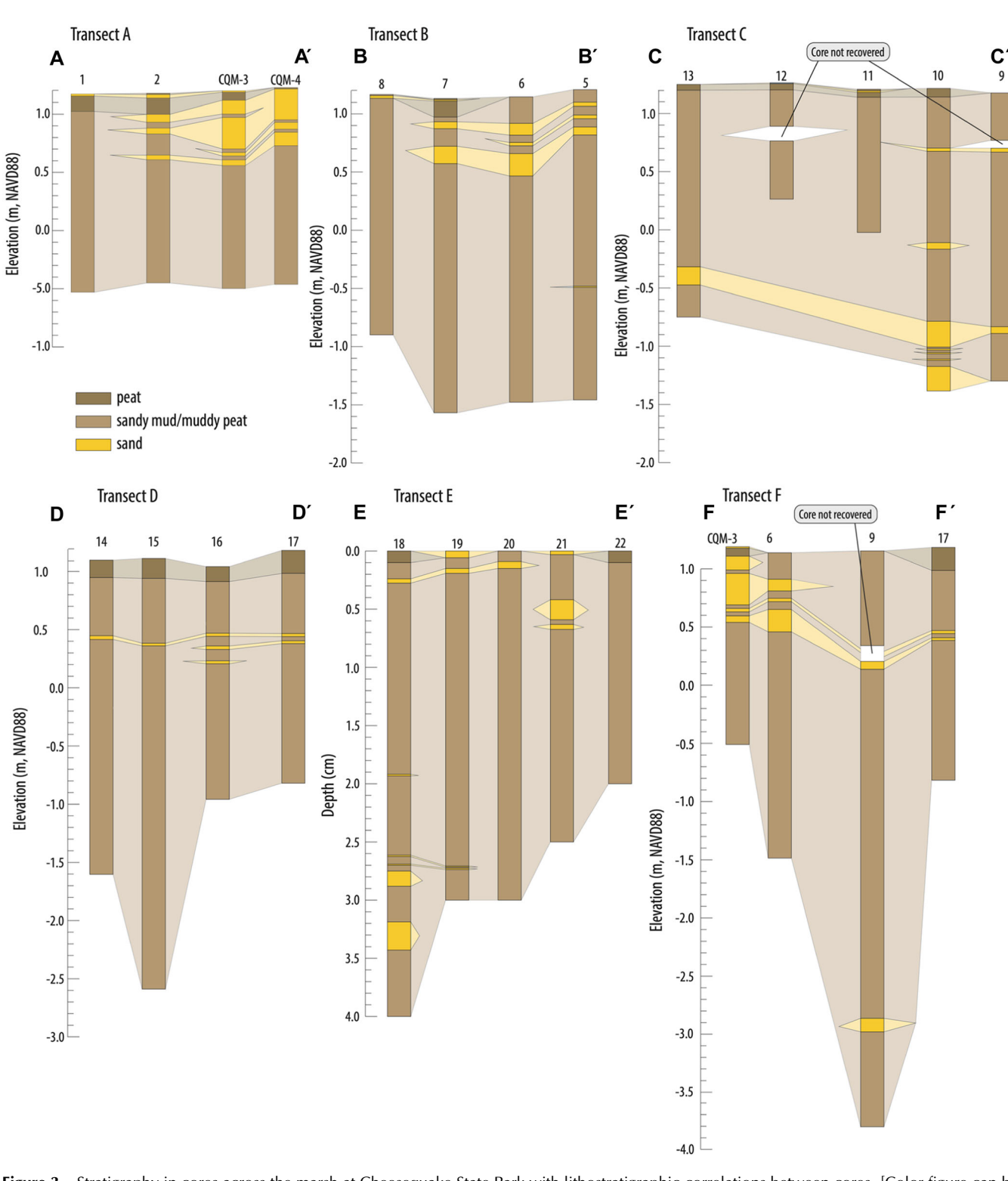


Figure 3. Stratigraphy in cores across the marsh at Cheesequake State Park with lithostratigraphic correlations between cores. [Color figure can be viewed at wileyonlinelibrary.com]

tion model for CQM-3 using the Bchron package in R (v.4.7.6, Haslett & Parnell, 2008). The timings of the modern chronohorizon inputs were assumed to originate from normal probability distributions. We ran Bchron for 200 000 iterations to produce age estimates for every 1-cm depth with 95% credible intervals (Haslett & Parnell, 2008).

Age-depth models assume constant sedimentation rates through time. This assumption is broken by the sporadic and instantaneous sedimentation that occurs during a storm surge event, which interrupts constant background sedimentation on a salt marsh. To determine how sedimentation of the overwash

deposits affected the age–depth model of CQM-3, we ran a sensitivity test comparing two cases of the age–depth model. In the first case, we assumed constant sedimentation rates throughout CQM-3, including through the depths of the overwash deposits. In the second case, we generated the age–depth model after subtracting the depths of the overwash sediments and adjusting the heights of the chronohorizons and radiocarbon ages, accordingly. We then added the thicknesses of the overwash deposits back, while keeping the age of the sediments constant throughout the deposit to simulate instantaneous sedimentation.

Results

Identifying and dating overwash deposits at Cheesequake Marsh

Modern sediments collected from Paul's Beach were composed of medium-grained sands with a mean grain size of 2.0 ϕ (250 μm). No foraminifera tests were found in the Paul's Beach sediments. Modern sediments collected from Stump Creek, on the other hand, were composed of silt with a much finer mean grain size of 6.3 ϕ (12.7 μm). A total of 60 tests of foraminifera dominated by Trochammina inflata were found within the Stump Creek sediments.

We visually identified eight stratigraphic units within the top 1.5 m of CQM-3 that we assume originated from storm overwash events. The overwash deposits were identified by their lithostratigraphy and supported by mean grain size. Lithostratigraphic correlation of these sand layers show they produce fan-shaped overwash deposits across the marsh. The layers of overwash sand deposits were found interbedded in salt marsh peat, silty peats and sandy muds across the marsh at Cheesequake State Park. We group these salt marsh sediments into two stratigraphic units based on their organic content and mean grain size and correlate the units across transects (Figure 3): (1) modern heavily rooted, brown peat that is generally found within the upper 20 cm of sediment, if present, with organic content ranging from 13 to 35% and a mean grain size ranging from 6.7 to 4.3 φ (9.6–50.8 μ m); and (2) gray to brown silt with intermittent fluctuations in levels of detrital organic matter and sand with organic content ranging from 1 to 22% and a mean grain size ranging from 6.5 to 3.7 ϕ $(11.0-76.9 \mu m)$ (Figure 3).

Grain size analysis of samples taken downcore of CQM-4 show excursions of coarser mean grain size compared to background peat and muddy peat sediments (Fig. S2). These coarser sediments are assumed to be overwash deposits originated from storm surge events. The mean grain size of the overwash deposits is 3.6 (82.5 μ m) \pm 0.8 ϕ , while the peat and muddy peats in the remainder of the core have a mean grain size of 5.5 (22.1 μ m) \pm 0.7 ϕ . The mean grain size and depths of the overwash deposits in CQM-4 are consistent with those of CQM-3. Therefore, we assume the overwash deposits are laterally continuous across cores and create a fan-shaped morphology. CQM-4 has more fluctuations in grain size downcore than CQM-3. While these fluctuations were not identified in lithostratigraphy, they demonstrate how fluctuations in grain size may exist even when not identified in lithostratigraphy.

During the year-long water level record from Cheesequake Creek (December 1975 to November 1976, NOAA, 2021), the highest gauge reading occurred on 10 August 1976 from a large rainfall event created by Hurricane Belle, which passed to the east of New Jersey (NOAA, 2021) (Fig. S1). No overwash deposit was created at the Cheesequake marsh as a result of the terrestrial rainfall flooding from Hurricane Belle. Another water level gauge record from the same time period from the much larger Raritan River, which opens to Raritan Bay roughly 4 km to the northwest of the mouth of Cheesequake Creek, shows several high-water level events that are not associated with any known storms in the region and are not found within the Cheesequake Creek record (NOAA, 2021). Therefore, we assume the smaller catchment size of Cheesequake Creek, compared to that of the Raritan River, limits the ability of terrestrial flooding events to create coarse-grained deposits throughout the Cheesequake marsh.

Comparisons of the two cases of our age-depth model (one run assuming constant sedimentation through time and one run assuming sporadic and instantaneous sedimentation from storm surges) show the deposition of overwash deposits does not affect the age—depth model of CQM-3 (Fig. S3). Therefore, we use the case assuming constant sedimentation to determine the ages of the overwash deposits (Figure 4).

Overwash deposits of CQM-3

Overwash Deposit 1

The uppermost overwash deposit was found at depths ranging from 1.11 to 1.23 m NAVD88 with thicknesses from 1 to 3 cm. Overwash Deposit 1 was found in cores along Transects A, B, C and E (Figure 3). The overwash deposit was thickest near Stump Creek and the southwestern half of the marsh (e.g. cores 2, 8 and 19) and decreased in thickness towards the coast to the northeast before pinching out 30-65 m along the transects. This overwash deposit is a sand (95% sand) that is sedimentologically distinct with a much coarser grain size $(2.4 \text{ }\phi/189\,\mu\text{m})$ and lower organic content (4.2%) than the overlying and underlying sediments (6.8 $\phi/9.0 \,\mu m$ and 34-35%, respectively) (Figure 5). Geochemical indicators of $\delta^{13} C$ and C/N measured within Overwash Deposit 1 (–21.7% and 5.2) did not differ from those in the underlying sediments (-20.8% and 6.8). The number of foraminifera specimens counted within the overwash deposit (144 tests per 5 cm³) was lower than the overlying and underlying sediment (1480 and 464 tests per 5 cm³, respectively) (Figure 6). The overwash deposit and the overlying and underlying sediment had the same foraminifera assemblage with high relative abundances of salt marsh foraminifera species Tr. inflata, Entzia macrescens and Arenoparrella mexicana. Overwash Deposit 1 was found at a shallower depth than any chronohorizons in CQM-3 (Figure 7).

Overwash Deposit 2

The second overwash deposit in CQM-3 was found at 23–24 cm depth. This overwash sand was found in cores along Transects A and B (and potentially Transect E) (Figure 3).

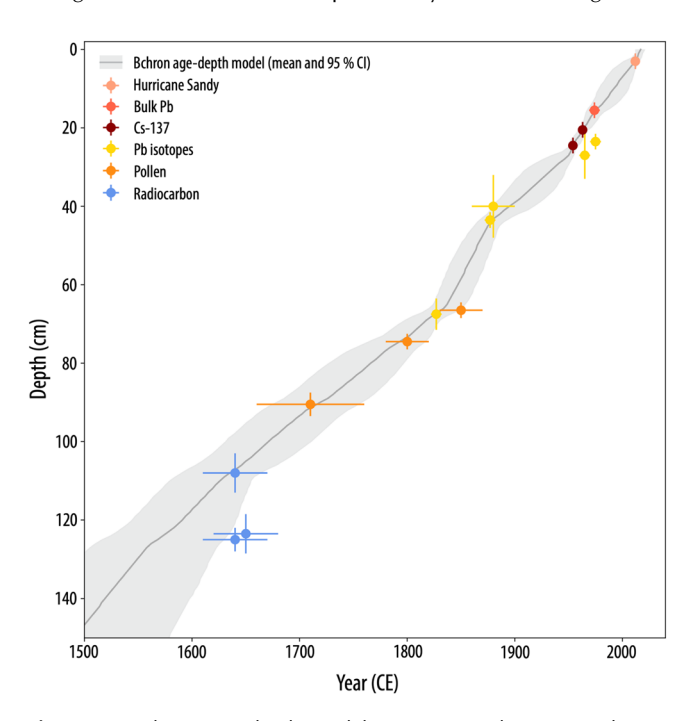


Figure 4. Bchron age–depth model estimates with mean and 95% confidence intervals. Colored markers indicate the timing and depth of chronohorizons used as input in the age–depth model with horizontal and vertical bars representing uncertainties in age and depth, respectively. [Color figure can be viewed at wileyonlinelibrary.com]

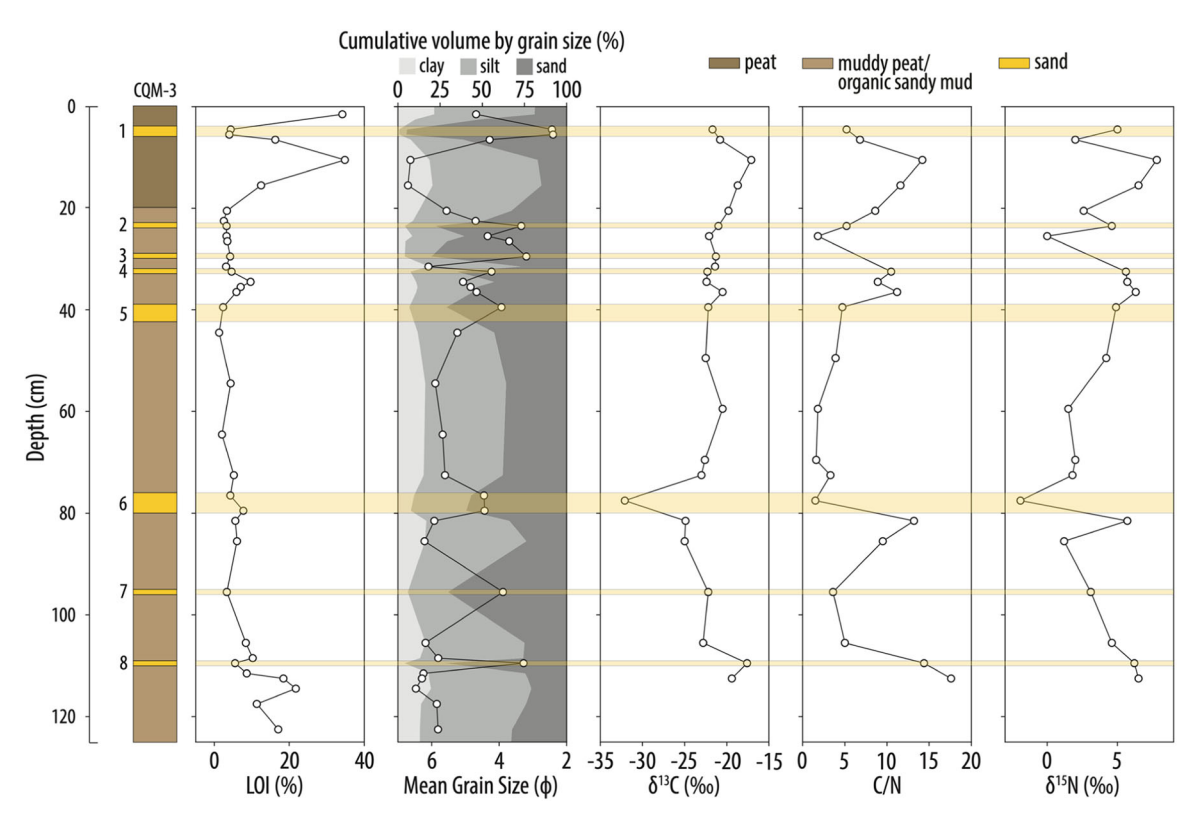


Figure 5. Sedimentary and geochemical data including loss-on-ignition (%), mean grain size (ϕ) , $\delta^{13}C$, C/N and $\delta^{15}N$ of samples taken from CQM-3. Yellow bands correspond to sand layers from overwash events. [Color figure can be viewed at wileyonlinelibrary.com]

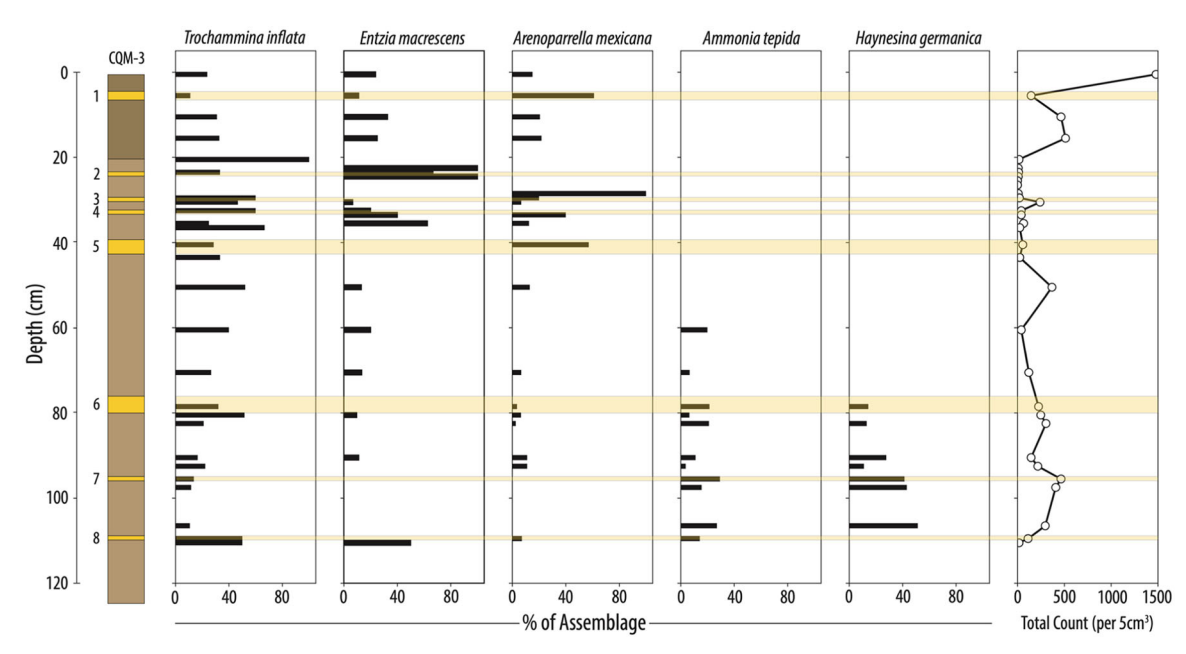


Figure 6. Foraminifera data including total counts and relative abundances of species of samples taken from CQM-3. Colors of stratigraphic units are consistent with Figure 5. [Color figure can be viewed at wileyonlinelibrary.com]

The overwash sand was not differentiable from other sand deposits in the field but was distinguished by grain size analysis. Stratigraphy shows the sands are thickest in cores proximal to the coast (e.g. cores 3, 4 and 6) and thin inland to the southwest before pinching out ~60 m along transects. Overwash Deposit 2 is a sand layer (78% sand) distinct from overlying and underlying sediments by grain size. The overwash deposit has a coarser mean grain size (3.3 $\phi/102\,\mu\text{m})$ than overlying and underlying sediments (4.7 and 4.3 $\phi/38.5$ and 50.8 μm , respectively) (Figure 5). Organic content measured via LOI was consistent at 2.5–3.3% across the

overwash deposit. Geochemical indicators showed no significant changes between the overwash deposit and surrounding sediments. Values of $\delta^{13}C$ were measured at -19.8 to -22.1% in the overlying and underlying sediments, while $\delta^{13}C$ within the overwash deposit was -21.0%. C/N values followed a decreasing trend across the deposit of 8.6, 5.2 and 1.8 above, at and below the deposit, respectively. Foraminifera were sparse (<12 tests per 5 cm³) and entirely composed of salt marsh species *E. macrescens* and *Tr. inflata* below the modern peat boundary at $\sim\!20$ cm depth (Figure 6). The foraminifera assemblage remained consistently sparse until $\sim\!30$ cm depth.

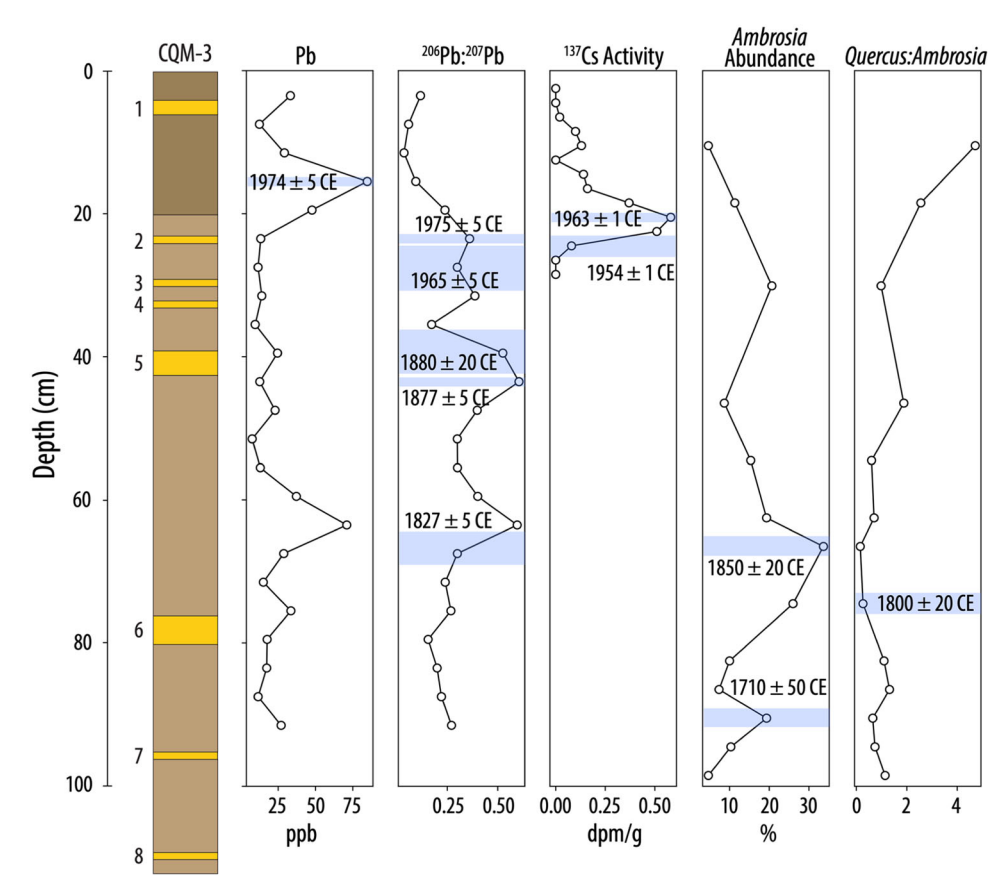


Figure 7. Levels of chronohorizons in samples collected from CQM-3 including levels of bulk Pb (ppb), ²⁰⁶Pb:²⁰⁷Pb, relative abundances of *Ambrosia* pollen, *Quercus:Ambrosia* counts, and levels of ¹³⁷Cs activity (dpm/g). Blue bars indicate changes in chronological proxies corresponding to anthropogenic activity. [Color figure can be viewed at wileyonlinelibrary.com]

Overwash Deposit 2 was found at the same depth of 23–24 cm as two chronohorizons found in CQM-3 including (1) a peak in $^{206}\text{Pb:}^{207}\text{Pb}$ dated to 1975 ± 5 CE and (2) an initial increase in ^{137}Cs dated to 1954 ± 1 CE (Figure 7).

Overwash Deposit 3

The next overwash deposit recorded in CQM-3 was found at a depth of 29-30 cm. This overwash deposit was found in cores from Transects A and B (and potentially Transect E) (Figure 3). In Transect A, the overwash deposit was not differentiated from other sand layers in field stratigraphy. Overwash Deposit 3 was more distinct in cores along Transect B, where it ranges in thickness from 2 to 3 cm in cores proximal to the coast (e.g. cores 5 and 6) before thinning and pinching off ~60 m inland to the southwest. Overwash Deposit 3 is a sedimentologically distinct sand (80% sand) with a coarser mean grain size (3.2 φ / 109 μ m) than surrounding sediments (6.1 and 3.7 ϕ /14.6 and 76.9 µm) (Figure 5). Organic content increased nominally in the overwash deposit to 4.2% from 3.1 and 3.5% in the underlying and overlying sediments, respectively. Indicators for δ^{13} C values showed no change between the surrounding sediments (-22.1 and -21.4%) and the overwash deposit (-21.3%). Foraminifera remained sparse (20 tests of Ar. mexicana, Siphotrocahmmina lobata and Tr. inflata per 5 cm³) in the overwash deposit and the overlying sediments (Figure 6). However, the total count of foraminifera specimens in the underlying sediments increased (240 tests per 5 cm³) and had high relative abundances from species Tr. inflata, Tiphotrocha comprimata, S. lobata and Haplophragmoides manilaensis. This overwash deposit occurs between two ²⁰⁶Pb:²⁰⁷Pb chronohorizons found in CQM-3 including (1)

an increase at 27 cm dated to 1965 ± 5 CE and (2) a decline found at 40 cm dated to 1880 ± 20 CE (Figure 7).

Overwash Deposit 4

The fourth overwash deposit captured in CQM-3 was found at a depth of 32-33 cm. This overwash deposit was found in cores along Transects A and B (Figure 3). The overwash deposit was not differentiable from other sand layers in field stratigraphy but was distinguished by grain size analysis. The thickness of the sand layers, including Overwash Deposit 4, was greatest in cores nearest to the coast (e.g. 3-6 and 9) before thinning landward towards Stump Creek and pinching out ~60 m along transects. Overwash Deposit 4 is a sedimentologically distinct sand layer (65% sand) (Figure 5). Mean grain size of the overwash sand layer, measured at $4.2 \, \phi$ (54.4 µm), exceeded that of underlying and overlying sediments (5.1 and 6.1 φ /29.2 and 14.6 μ m, respectively). Organic content was consistent at 3.1-4.6% across the contact separating the overwash deposit from overlying sediments. A small peak in organic content to 9.7% was found in the sediments underlying the overwash deposit at a depth of 34–35 cm. The δ^{13} C value of Overwash Deposit 4 (–22.3‰) did not differ from those measured in sediments above and below the overwash deposit (-21.4 and -22.4%, respectively). C/N values did not differ between the overwash deposit and underlying sediments (10.5 and 8.9, respectively). Foraminifera consisting of Ar. mexicana, E. macrescens, Ti. comprimata and Tr. inflata were sparse (40 tests per 5 cm³) within the overwash deposit and within underlying sediments (Figure 6). The layer of sediment overlying the overwash deposit contained higher numbers of salt marsh foraminifera (240 tests per 5 cm³) consisting of *Ti. comprimata* and *Tr.*

inflata specimens. This overwash deposit is found between the same ²⁰⁶Pb:²⁰⁷Pb chronohorizons as Overwash Deposit 3 in CQM-3 (Figure 7).

Overwash Deposit 5

A fifth overwash deposit captured by CQM-3 was found at a depth of 39-43 cm. This overwash deposit is found in Transects A and B but was not differentiable from overlying sand layers in the field but followed the landward-thinning morphology of younger deposits (Figure 3). Overwash Deposit 5 is a sand layer (71% sand) that is distinct from overlying and underlying sediments by mean grain size (Figure 5). Mean grain size increased from 5.2 ϕ (27.2 μ m) in the sediments underlying the overwash deposit, to 3.9 φ (67.0 μ m) within the overwash sand, and decreased again to 4.7 ϕ (38.5 μ m) in the sediments overlying the overwash deposit. Organic content did not change between the overwash deposit (2.3%) and the underlying sediments (1.3%). Values of δ^{13} C remained consistent from -22.5% below the overwash deposit, to -22.2% within Overwash Deposit 5, to -20.5% above the overwash deposit. C/N values increased slightly from 4.7 and 3.9 within and below the overwash deposit, respectively, to 11.2 in sediments overlying the overwash deposit. Foraminifera were sparse within this overwash layer (56 tests per 5 cm³) and within the surrounding sediments (24 tests per 5 cm³ above and below the overwash deposit) (Figure 6). The species with the highest relative abundances in the overwash deposit and the overlying sediments include Hap. manilaensis and Tr. inflata. However, the overwash deposit also saw an increase in the relative abundance of Ar. mexicana specimens compared to the overlying sediments. The sediments below the overwash deposit had an assemblage consisting of marine calcareous Elphidium sp. and, to a lesser extent, Tr. inflata. This overwash deposit occurs at the same depth as the decline in ²⁰⁶Pb:²⁰⁷Pb, which was correlated to an age of 1880 ± 20 ce (Figure 7).

Overwash Deposit 6

One of the thickest overwash deposits in CQM-3 was found at a depth of 76-80 cm. This sand layer was found in cores along Transect A, and sand layers at similar depths were found in cores along Transects D and E (Figure 3). However, without dating these cores, validating the correlation of the overwash sand across transects is uncertain. Along Transect A, the morphology of Overwash Deposit 6 followed that of Overwash Deposits 2-5. Overwash Deposit 6 is a sand layer (60% sand) that is sedimentologically differentiable from overlying and underlying sediments by grain size analysis (Figure 5). Mean grain size throughout the sand layer was consistent at 4.4 φ (47.4 μ m), while mean grain size of the underlying and overriding sediments were finer at 5.9 and 5.6 φ (16.7 and 20.6 µm), respectively. Organic content increased slightly within the overwash layer with depth from 4.3 to 7.7%, while the organic content of the sediments in which the overwash deposit was embedded had a consistent organic content of 5.2-5.6%. Overwash Deposit 6 displayed a negative excursion in δ^{13} C at -32.1% compared to surrounding sediments, which had a range of -23.0 to -24.9%. C/N values of the overwash

deposit decreased to 1.5 relative to surrounding sediments (3.3–13.2). The foraminifera assemblage of Overwash Deposit 6 had a higher count (224 tests per 5 cm³) and a higher species diversity than any of the younger deposits (Figure 6). Species making up most of the assemblage include salt marsh species Tr. inflata and marine calcareous species Haynesina germanica, Haynesina depressula, Elphidium sp. and Ammonia tepida. Foraminifera were also present in the sediments surrounding the overwash deposit (120 and 248 tests per 5 cm³). Species with the highest relative abundances in these sediments include E. macrescens, Lepidodeuteammina ochracea, and Tr. inflata. The overwash deposit lies between two pollen chronohorizons; the chronohorizons include the ratio of Quercus to Ambrosia pollen falling below 1.0 found at 74–75 cm and dated to 1800 ± 20 CE and the initial rise in Ambrosia pollen found at 90–91 cm and dated to 1710 ± 50 CE (Figure 7).

Overwash Deposit 7

A seventh overwash deposit not identified within the stratigraphy in the field was found via grain size analysis in CQM-3 at a depth of 95-96 cm. Overwash deposits are found at similar depths in cores along Transects C and D but cannot be unequivocally correlated to Overwash Deposit 7 without chronological analyses of those cores (Figure 3). Because this overwash deposit was not identified as a unit in the field, its morphology across the marsh is unknown. Overwash Deposit 7 is a sand layer (70% sand) that was differentiable from surrounding sediments by grain size analysis. Mean grain size of the overwash deposit was much coarser (3.9 φ /67.0 μ m) than the sediments in which the deposit is embedded (6.2 φ / 13.6 µm below and above the deposit) (Figure 5). Organic content of the overwash deposit (3.3%) was slightly lower than that of the surrounding unit (6.0-8.4%). The value of δ^{13} C measured within the overwash deposit (-22.2%) was slightly heavier than overlying and underlying sediments (-25.0 and -22.8‰, respectively). C/N values were slightly lower in the overwash deposit (3.6) than in surrounding sediments (5.0-9.5). Foraminifera including Hay. germanica and Am. tepida made up the highest relative abundances of the 464 tests per 5 cm³ counted in Overwash Deposit 7 (Figure 6). Sediments overlying the overwash deposit had higher relative abundances of salt marsh foraminifera species including Tr. inflata, Ti. comprimata and S. lobata within their 216 tests per 5 cm³. Sediments underlying the overwash deposit, on the other hand, had a similar assemblage to Overwash Deposit 7 with 408 tests per 5 cm³. This overwash deposit lies between the initial rise in Ambrosia pollen found at 90-91 cm and dated to 1710 ± 50 CE and the radiocarbon-aged sample found at 108 cm and dated to 1640 ± 30 CE (Figure 7 and Table 2).

Overwash Deposit 8

The oldest overwash deposit captured in CQM-3 was found at a depth of 109–110 cm. Like Overwash Deposit 7, this sand layer was not identified as a distinct unit during field work but was later found via sedimentological analyses. Sand layers at similar depths are found in cores along Transects C and D, but

Table 2. Radiocarbon sample depths and ages. All samples were dated by Beta Analytic.

CQM-3 depth (cm)	Laboratory no.	Radiocarbon age (14C a)	Calibrated age (calendar a BP $\pm 2\sigma$)	δ ¹³ C (‰, VPDB)	Dated material
108	Beta-630479	310 ± 30	356 ± 56 347.5 ± 80.5 381 ± 81	-13.7	Wood
123.5	Beta-630475	300 ± 30		-13.1	Wood
125	Beta-630477	310 ± 30		-13.4	Wood

the relationship of Overwash Deposit 8 to these sand layers is unknown (Figure 3). The morphology of this overwash deposit is also unknown. Overwash Deposit 8 is a sand layer (72% sand) that was differentiated from surrounding sediments by grain size analysis (Figure 5). Mean grain size of the overwash deposit increased from 6.2φ (13.6 µm) within the underlying sediments, to 3.3 φ (102 µm) within the overwash layer, and decreased again to 5.8 φ (17.9 μ m) in the overlying organic sediments. Organic content decreases slightly from 8.6% in the underlying sediments, to 5.5% in the overwash deposit, before increasing to 10.3% in the overlying sediments. Geochemical indicators of $\delta^{13}C$ and C/N measured in Overwash Deposit 8 (-17.6% and 14.4) differed slightly from those measured in overlying (-22.8% and 5.0) and underlying sediments (-19.4% and 17.6). The foraminifera assemblage of Overwash Deposit 8 was composed of the salt marsh species Tr. inflata and Ti. comprimata, with a smaller component of the marine calcareous species Am. tepida (112 tests per 5 cm³) (Figure 6). The sediment overlying the overwash deposit had a higher relative abundance of marine calcareous species including Hay. germanica within its 296 tests per 5 cm³, while the sediment underlying the overwash deposit had very few specimens (16 tests per 5 cm³), which were entirely made up of Tr. inflata and E. macrescens. This overwash deposit lies between two radiocarbon-aged samples found in CQM-3 at 108 cm dated to 1640 ± 30 CE and 123-124 cm dated to 1650 ± 30 CE (Table 2).

Discussion

Characteristics of overwash deposits

We rely on the fan-shaped morphology and coarser mean grain size to classify the sand layers as overwash deposits at Cheesequake State Park in northern New Jersey. Overwash deposits found in back-barrier marsh environments have a documented fan-shaped morphology (e.g. et al., 2001b, Scileppi and Donnelly, 2007, Williams, 2009). The sand layers found in CQM-3 follow the expected fanshaped morphology of an overwash deposit where they are thickest near the coast to the northeast of the marsh and thin landward to the southwest (Figure 3). The exception is the uppermost overwash deposit from Hurricane Sandy. This overwash deposit is thickest towards the southwest and thins across the marsh to the northeast. Eyewitnesses observed Hurricane Sandy's storm surge flooding and overtopping the banks of Stump Creek to the southwest of the marsh rather than overtopping the coastal dunes to the northeast. Given that Hurricane Sandy's overwash deposit is composed of fine sands $(2.4 \,\varphi)$ and is dominated by *Tr. inflata* foraminifera, we believe the storm surge suspended and transported foreshore sediments through the mouth of Cheesequake Creek and into Stump Creek.

Overwash deposits have a characteristically coarser grain size than the back-barrier sediments in which they are embedded, as overwash sediments typically originate from foreshore environments and are transported by high-energy storm surges (e.g. Brandon et al., 2014, Bregy et al., 2018, Castagno et al., 2021). Modern analogue studies have demonstrated overwash deposits of known storms possess coarser grain sizes than underlying sediments (e.g. Hawkes and Horton 2012, Brandon et al., 2014, Hong et al., 2018). For example, Soria et al. (2017) described the sedimentological characteristics of Typhoon Haiyan's overwash deposit at sites along the coast of Leyte Gulf, Philippines, after the storm made landfall on Leyte Island in 2013. The overwash deposit left by

Typhoon Haiyan had a larger mean grain than pre-Haiyan soils throughout both a mixed siliciclastic–carbonate and a carbonate-rich coast (Soria et al., 2017). Grain size was similarly successful at distinguishing eight overwash events in CQM-3 from autochthonous coastal sediments (Figure 5). The overwash sediments in CQM-3 had a mean grain size of 3.6 (82.5 µm) \pm 0.7 ϕ , while autochthonous coastal sediments had a finer mean gain size of 5.6 (20.6 µm) \pm 0.8 ϕ . The coarser mean grain size of the overwash deposits in CQM-3 is consistent with that of modern sediments collected at Paul's Beach (2.0 $\phi/250\,\mu\text{m}$). The similarity in mean grain size between the overwash deposits and modern beach sediments supports the sediment source of the overwash deposits originating from the foreshore.

The organic content of overwash deposits is lower than that of the back-barrier sediments in which they are found given the high minerogenic content of nearshore source environments compared to the high organic contents of back-barrier environments (e.g. Donnelly et al., 2004, Hawkes and Horton, 2012, Soria et al., 2017). Organic content has been used to differentiate overwash deposits from autochthonous, back-barrier sediments in modern analogue and paleo-overwash studies (e.g. Kiage et al., 2011, Horton et al., 2009, Joyse et al., 2023). For example, Hawkes and Horton (2012) found overwash sediments from Hurricane Ike on Galveston and San Luis Islands, Texas, had a lower organic content than underlying pre-storm sediments. However, organic content was only successful at distinguishing the overwash sediments of Hurricane Sandy and Overwash Deposit 8 in the organic-rich sections of CQM-3, including the top 20 cm of peat and the lower 15 cm of muddy peat (Figure 5). In the intermediary clastic-rich sections of the core, the overwash deposits did not differ in organic content from the autochthonous coastal sediments.

Geochemical indicators, including δ^{13} C and C/N, have the potential to record a marine signature from extreme flooding events from storms and tsunamis (e.g. Lambert et al., 2008, Pilarczyk et al., 2012, Das et al., 2013). These proxies capture the isotopic signature of marine organic matter, which often differs from that of terrestrial organic matter such that δ^{13} C signatures are generally higher in marine organic matter versus terrestrial organic matter (e.g. Lambert et al., 2008, Pilarczyk et al., 2012, Das et al., 2013). However, the geochemical indicators from CQM-3 did not display evidence of marine inundation (Figure 5). The overwash layers found in CQM-3 had no positive excursion in δ^{13} C or decrease in C/N values compared to the surrounding back-barrier sediments. The lack of excursions in the geochemical indicators from CQM-3 could come from the fact that the Cheesequake salt marsh is not isolated from marine inundation. Rather, the salt marsh, which is located ~0.5 km from the mouth of Raritan Bay, is inundated daily by tidal creek flooding from Stump Creek. Therefore, the $\delta^{13}C$ and C/N values within the salt marsh sediments probably come from a combination of marine and terrestrial origins, and this dual origin masks the marine signal of the overwash sediments.

Foraminiferal assemblages have been successfully used in paleo-storm and modern analogue studies to identify the marine provenance of overwash sediment from the brackish to terrestrial signal of back-barrier sediments (e.g. Hippensteel and Martin, 1999, Hawkes and Horton, 2012, Pilarczyk et al., 2016). For example, the foraminiferal assemblage of Typhoon Haiyan's overwash deposit along the Leyte and Samar coasts in the Philippines contained a high abundance of marine calcareous foraminifera, which were absent from underlying soils (Pilarczyk et al., 2016). Additional studies have shown foraminifera have difficulty providing proxy evidence of extreme overwash events due to bioturbation

and low rates of preservation (e.g. Williams, 2010, Hippensteel, 2011, Hippensteel and Garcia, 2014). The sandy layers found in CQM-3 align with the results of studies such as Hippensteel and Garcia, (2014) and Horton et al. (2009), the latter of which found an absence of foraminifera in the overwash sediments of Hurricanes Katrina and Rita in salt marshes along the Louisiana and Alabama coastlines. Sand layers within CQM-3 that occur above ~40 cm, including Overwash Deposits 1-5, have nominal counts of agglutinated salt marsh foraminifera species such as Tr. inflata, E. macrascens and Ar. mexicana (Figure 6). Sediments below 40 cm display an increase in the diversity and abundance of foraminifera present. Overwash Deposits 6 and 7 contain an increase in calcareous marine foraminifera species such as Am. tepida, Hay. germanica and Elphidium sp. over the sediments in which they are embedded. However, the foraminifera assemblage of Overwash Deposit 8 is again dominated by agglutinated salt marsh foraminifera Tr. inflata and Ti. comprimata. Modern sediment sampled from the beach northeast of the marsh likewise contained no foraminifera tests, while sediment taken from Stump Creek contained 60 tests dominated by Tr. inflata specimens. Given the absence of calcareous marine foraminifera from most of the sand layers and from the modern beach sediments, we cannot ascertain the marine source of overwash deposits in CQM-3 from foraminifera. However, the presence of Tr. inflata in several of the overwash deposits is consistent with the foraminiferal assemblage of modern sediments collected from Stump Creek, which suggests the storm surges that created these overwash deposits also flooded the marsh via Stump Creek.

The sensitivity of the geologic record in preserving overwash deposits is temporally variable as the coast responds to geomorphological processes through time (Donnelly and Webb, 2004, Liu, 2004, Wallace et al., 2014). Variations in (1) the height and width of the coastal barrier, (2) the configuration of tidal channels and inlets, (3) the height of relative sea level and/or (4) the distance of the coastal barrier to the marsh can all alter the likelihood of overwash sediments being deposited and preserved in the geologic record (e.g. Donnelly, et al., 2001b, Scileppi and Donnelly 2007). For example, Mattapoisett Marsh, MA, has preserved a relatively high-resolution record of overwash events, with 30 overwash deposits over the last 2000 years, compared to other back-barrier environments in the northeastern US (Boldt et al., 2010). Boldt et al. (2010) suggest the higher sensitivity of the site may be attributed to the lower height of the barrier. Aerial images and historical maps show little morphological changes to the Cheesequake marsh over the instrumental time period beyond the reconfiguration of Stump Creek with the addition of access roads to Route 35 between 1943 and 1954 (U.S. Geological Survey, 1943, 1954).

Storm deposits at Cheesequake

We reconstructed the paleo-storm history at a back-barrier marsh in Cheesequake State Park in northern New Jersey. This geologic reconstruction extends the record of landfalling cyclone activity in the region by ~300 years beyond instrumental tide gauge records. Eight and 11 major water level events have been recorded above the 10% AEP level at the Sandy Hook and Battery tide gauges, respectively. Of these events, only four were also captured by the geologic record at Cheesequake. Therefore, we can conclude the geologic record at the Cheesequake marsh has a 36–50% preservation rate of extreme water level events in excess of the 10% AEP of occurrence level. This indicates that estimates of extreme water level return periods from the geologic record at Cheesequake marsh could underestimate the true value of those return

periods without considering the preservation bias of the geologic record.

Overwash Deposit 1 is assumed to have resulted from Hurricane Sandy's flooding of the Cheesequake salt marsh based on eyewitness accounts of Hurricane Sandy's storm surge. Additionally, Hurricane Sandy produced the highest water levels ever recorded at the Sandy Hook and the Battery tide gauges at 2.7 m above MHHW (NOAA, 2021) (Table 1). Sedimentological evidence of Hurricane Sandy's overwash event has been found in cores obtained from Seguine Pond on the southern coast of Staten Island, New York (Brandon et al., 2014), and from Fire Island, New York (La Selle et al., 2017). Brandon et al. (2014) found Hurricane Sandy's overwash deposit was the second coarsest event deposit found at Seguine Pond, behind an overwash deposit produced by an 1821 CE hurricane. The increase in mean grain size and D_{90} recorded in Hurricane Sandy's deposit at Seguine Pond (Brandon et al., 2014) is consistent with the coarsening observed in Hurricane Sandy's deposit relative to surrounding sediments at Fire Island (La Selle et al., 2017) and in CQM-3.

Historical storms that occurred during the estimated age interval for Overwash Deposit 2 of 1963–1952 cε (2σ) and produced extreme water levels at the Sandy Hook and Battery tide gauges include (1) the Ash Wednesday Nor'easter of 1962, (2) Hurricane Donna in 1960 and (3) a 1953 Nor'easter (Table 3). Estimates from our age-depth model preclude the landfall of Hurricane Belle in 1976, which made the highest water level record at the brief Cheesequake Creek tide gauge from high rainfall and terrestrial flooding (Table 3). Hurricane Donna, on the other hand, held the highest water level record at the Battery tide gauge at 1.5 m above MHHW prior to Hurricane Sandy in 2012 (Brandon et al., 2014). Hurricane Donna's overwash deposit has been identified via its coarser grain size compared to surrounding sediments in cores taken north of Cheesequake State Park at Seguine Pond, New York (Brandon et al., 2014), and from Mattapoisett Marsh, Massachusetts (Boldt et al., 2010, Castagno et al., 2021).

Paleo-overwash studies from back-barrier marshes in southern New Jersey find small overwash fans that are attributed to the 1962 Ash Wednesday Nor'easter rather than Hurricane Donna (Donnelly et al., 2004). The attribution of the southern NJ overwash deposits to the Ash Wednesday storm over Hurricane Donna originates from the fact that the Ash Wednesday storm produced an extreme water level record at the nearby Atlantic City tide gauge, while Hurricane Donna did not (Donnelly et al., 2004; NOAA 2021). Based on the relative magnitudes of the extreme water levels associated with the three candidate storms, we attribute Overwash Deposit 2 to Hurricane Donna.

Overwash Deposit 3 has an estimated age between 1919 and 1951 \subset (2 σ) (Table 1), and two of the most extreme water level events recorded by the Sandy Hook tide gauge fall within these age bounds, including a 1950 Nor'easter and the 1944 Great Atlantic Hurricane (Table 3). An unnamed hurricane from 1938 that produced an extreme water level record at the Battery tide gauge also falls within the age bounds of the age-depth model. Sedimentary records of the 1944 Great Atlantic Hurricane have been identified in cores from Mattapoisett Marsh, Massachusetts (Boldt et al., 2010, Castagno et al., 2021), and were suspected to be captured in a back-barrier marsh in Brigantine, New Jersey (Donnelly et al., 2004). However, without aerial photographs from 1941 to 1950 CE, Donnelly et al. (2004) were not able to determine if the Great Atlantic Hurricane of 1944, the 1950 Nor'easter or both were responsible for breaching the barrier at Brigantine.

The 1938 hurricane did not produce a water level record above the 10% AEP water level height at the Sandy Hook tide gauge (NOAA, 2021). While the storm did produce a more

Table 3. Overwash deposits within CQM-3 and corresponding age constraints (2σ) from the Bchron age–depth model with a list of corresponding storms that produced extreme sea-level events at the Sandy Hook tide gauge or found in regional paleo-storm proxy records that fall within the uncertainty bounds of the age–depth model.

Overwash deposit	Bchro			
	Minimum age (CE)	Mean age (CE)	Maximum age (CE)	Possible overwash events
1		2012		Hurricane Sandy 2012
2	1952	1957	1963	Nor'easter 1962
				Donna 1960
				Nor'easter 1953
3	1919	1941	1951	Nor'easter 1950
				Hurricane 1944
				Hurricane 1938
4	1905	1929	1946	Hurricane 1944
				Hurricane 1938
5	1874	1893	1923	Hurricane 1893
6	1773	1 <i>777</i>	1810	Hurricane 1821*
				Hurricane 1788
7	1651	1693	1731	Hurricane 1693
8	1584	1630	1658	

^{*}Hurricane 1821 falls outside of the age-depth model's 2σ age constraints for Overwash Deposit 6.

significant water height of 0.8 m above MHHW at the Battery tide gauge, the storm is not within the top ten most extreme water level events captured at the tide gauge (NOAA, 2021). Despite the small surge produced by the storm, the overwash deposit from the 1938 Hurricane has been documented in coastal salt marshes from the mid-Atlantic to southern New England (e.g. Donnelly et al., 2004; Boldt et al., 2010; Maio et al., 2016; Castagno et al., 2021).

Overwash Deposit 4 has an estimated age between 1905 and 1946 ce (2 σ). Two hurricanes that potentially produced Overwash Deposit 3, including the Great Atlantic Hurricane of 1944 and the Unnamed 1938 Hurricane, also fall within the age–depth model's estimates for the age of Overwash Deposit 4 (Table 3).

Overwash Deposit 5 has an estimated age between 1874 and 1923 CE (2σ) (Table 3). The only historical storm that falls within this age range and has a documented storm track within 30 km of the study site is an 1893 hurricane (NOAA, 2022). The storm is reported to have produced an estimated 1.6-m storm tide in New York Harbor from archived tide gauge data (Talke et al., 2014). An overwash deposit from the 1893 hurricane is notably missing from geologic overwash records from southern New Jersey (Donnelly et al., 2004) and from Staten Island, New York (Brandon et al., 2014). However, an overwash deposit found in salt marshes in southwestern Long Island, New York, has been attributed to the hurricane (Scileppi and Donnelly,, 2007). These neighboring paleo-records do not report any other storms that fall within the age constraints of the age-depth model that could be attributed to Overwash Deposit 5. Overwash Deposit 5 is also one of the thickest overwash deposits found in CQM-3 at 4-cm thickness, which is in stark contrast to nearby records where the deposit is not recorded.

Overwash Deposit 6 has an estimated age between 1773 and 1810 ce (2σ) (Table 3). This overwash deposit was probably produced by a major hurricane that tracked northeast across the states of New Jersey and New York into western New England in mid-August 1788 ce (Ludlum, 1963, Scileppi and Donnelly, 2007). Boose et al. (2001) estimate the 1788 hurricane was a Category 3 storm at landfall, and the storm surge in New York City is estimated to have been 3 m relative to MSL (~2.2 m above MHHW) (Donnelly et al., 2004, Scileppi and Donnelly, 2007). Sedimentary records from the 1788 hurricane are found in back-barrier salt marshes in New York and southern New England (Scileppi and Donnelly, 2007, Brandon et al., 2014). Donnelly et al. (2004) also found evidence of a

pre-instrumental storm in southern New Jersey that could be attributed to the 1788 hurricane or a later hurricane that made landfall in 1821. Age constraints were not able to resolve which of the two hurricanes (or if both) produced the observed southern New Jersey overwash deposit (Donnelly et al., 2004).

Our age-depth model excludes the 1821 hurricane from its 2σ uncertainty estimates, making the 1788 hurricane the more likely source of the deposit, assuming our age-depth model is accurate. However, it is important to note historical documents show the 1821 hurricane produced extensive damage and flooding throughout New Jersey, New York City and Long Island, New York (Ludlum, 1963). As previously mentioned, the 1821 hurricane is also attributed to the coarsest overwash deposit found at Seguine Pond, which is located across Raritan Bay from the Cheesequake marsh (Brandon et al., 2014). Given the coarse grain size of the 1821 storm's overwash deposit compared to Hurricane Sandy's in 2012, it is estimated that the 1821 storm was of similar strength to Hurricane Sandy and produced an even larger storm surge (Brandon et al., 2014). Therefore, it is difficult to exclude the possibility that Overwash Deposit 6 is not partly (in conjunction with the 1788 storm) or entirely a result of the 1821 storm. A more reasonable explanation may be that the 1821 hurricane is a candidate for producing Overwash Deposit 6, and the age-depth model is slightly biased at depth where larger uncertainties occur.

Overwash Deposit 7 has an estimated age of 1651 to 1731 ce (2 σ) (Table 3), and a 1693 hurricane is the only documented historical storm that occurs during this time period. This storm produced changes in rivers and coastlines from Virginia to Long Island, New York, in late October 1693 (Ludlum, 1963). Overwash deposits in back-barrier marshes on Staten Island and Long Island, New York, found via anomalies in grain size have been correlated to the 1693 hurricane (Scileppi and Donnelly, 2007, Brandon et al., 2014).

The final and oldest overwash deposit found in CQM-3 has an estimated age of 1584–1658 ce (2 σ) (Table 3) and pre-dates all the historical and instrumental records from the region and, therefore, originated from a pre-historic storm.

Conclusion

Geologic records can be used to extend records of landfalling storm activity beyond instrumental and historical periods.

10991417, 0, Downloaded from https://onlinelibrary.wiley.com/doi/10.1002/qs.3622 by Rutgers University Libraries, Wiley Online Library on [29/052024]. See the Terms and Conditions (https://onlinelibrary.wiley.com/rems-and-conditions) on Wiley Online Library for rules of use; OA articles are governed by the applicable Creative Commons Licenses

However, understanding the preservation potential of geologic records is essential to accurately determine the return periods of extreme water level events from storms. Anthropogenic land use changes in urban areas have made it increasingly difficult to find and produce geologic storm records in these regions.

From a back-barrier salt marsh at Cheesequake State Park in northern New Jersey, we identified eight overwash deposits from extreme flooding events and constrained the ages of those deposits to the timing of known coastal storms in instrumental and historical records. In doing so, we found:

- Overwash deposits were identifiable by their fan-shaped morphology and anomalously coarser grain size compared to the back-barrier sediments in which they were embedded, as supported by the mean grain sizes of modern beach sediments.
- Extreme coastal storm flooding can originate from tidal creeks as well as from the coast as seen with Hurricane Sandy's overwash deposit, which originated from Stump Creek. This is further supported by the dominance of *Tr. inflata* in many of the overwash deposits and in modern sediments collected from Stump Creek.
- Organic content, geochemical indicators and foraminiferal assemblages of the overwash sediments were unable to verify a marine provenance for the overwash deposits.
- The geologic record at Cheesequake was able to extend the record of landfalling cyclone activity by ~300 years beyond instrumental records in the region.
- Age-depth modeling coupled with neighboring tide gauge and paleo-storm records constrained the age of the seven pre-Sandy overwash deposits such that each deposit was attributable to one to three storms.

Based on the four overwash deposits found within the overlapping time period between the Sandy Hook and Battery tide gauges and the Cheesequake geologic record, we conclude the geologic record at Cheesequake has a 36–50% preservation rate of extreme sea-level events above the 10% AEP of exceedance level calculated from tide gauge data. This has implications for return intervals determined based on geologic records in the region in that those records may underestimate the true number of extreme water level events.

Acknowledgements. KMJ would like to thank Christian Rowan, Ashlyn Spector, J. N. Stanle, and John Schmelz for their assistance with field work and data collection. KMJ and REK were supported by grants from the US National Science Foundation (DGE-1633557, ICER-1663807, OCE-1804999, ICER-2103754, the last as part of the Megalopolitan Coastal Transformation Hub). KMJ, TAS and BPH were funded by the Ministry of Education Academic Research Fund MOE2019-T3-1-004. This work is Earth Observatory of Singapore contribution 598. The authors acknowledge PALSEA, a working group of the International Union for Quaternary Sciences (INQUA) and Past Global Changes (PAGES), which in turn received support from the Swiss Academy of Sciences and the Chinese Academy of Sciences.

Data availability statement

The data that support the findings of this study are openly available in The geologic record of extreme storm events from New Jersey at https://doi.org/10.21979/N9/6JKDVG.

Supporting information

Additional supporting information can be found in the online version of this article.

Figure S1. Hourly tide gauge data from Cheesequake Creek in green and Raritan River in blue.

Figure S2. Mean grain size (ϕ) comparison from CQM-3 and adjacent core CQM-4. Yellow bars indicate overwash layers identified in CQM-3.

Figure S3. Bchron age–depth model results with 2σ uncertainty levels. Colored markers indicate the timing and depth of chronohorizons used as input in the age–depth model with horizontal and vertical bars representing uncertainties in age and depth, respectively. Gray curve shows model results when continuous sedimentation is assumed (primary model used in text), and green curve shows model results when instantaneous sedimentation from storm surges is assumed.

Abbreviations. AEP, annual expected probability; ETC, extratropical cyclone; GIA, glacio-isostatic adjustment; LOI, loss on ignition; MHHW, mean higher high water; RSLR, relative sea-level rise; TC, tropical cyclone.

References

- Bennett, K.D. & Willis, K.J. (2002) Pollen. In: Smol, J.P., Birks, H.J. & Last, W.M., (Eds.) *Tracking Environmental Change Using Lake Sediments: Volume 3:Terrestrial, algal, and siliceous indicators,* 3. Springer Science and Business Media.
- Blake, E.S., Kimberlain, T.B., Berg, R.J., Cangialosi, J.P., Beven II, J.L., & National Hurricane Center, (2013). *Tropical Cyclone Report Hurricane Sandy* (No. AL182012; pp. 1–157). National Hurricane Center.
- Blott, S.J. & Pye, K. (2001) Gradistat: A grain size distribution and statistics package for the analysis of unconsolidated sediments. *Earth Surface Processes and Landforms*, 26, 1237–1248.
- Boldt, K.V., Lane, P., Woodruff, J.D. & Donnelly, J.P. (2010) Calibrating a sedimentary record of overwash from Southeastern New England using modeled historic hurricane surges. *Marine Geology*, 275, 127–139.
- Boose, E.R., Chamberlin, K.E. & Foster, D.R. (2001) Landscape and regional impacts of hurricanes in New England. *Ecological Monographs*, 71(1), 27–48.
- Brandon, C.M., Woodruff, J.D., Donnelly, J.P. & Sullivan, R.M. (2014) How Unique was Hurricane Sandy? Sedimentary Reconstructions of Extreme Flooding from New York Harbor. *Scientific Reports*, 4, 7366.
- Bregy, J.C., Wallace, D.J., Totten, R.L. & Cruz, V.J. (2018) 2500-year paleotempestological record of intense storms for the northern Gulf of Mexico, United States. *Marine Geology*, 396, 26–42.
- Castagno, K.A., Donnelly, J.P. & Woodruff, J.D. (2021) Grain-Size Analysis of Hurricane-Induced Event Beds in a New England Salt Marsh, Massachusetts, USA. *Journal of Coastal Research*, 37(2), 326–335.
- Christie, M., Bernhardt, C., Parnell, A., Shaw, T., Khan, N., Corbett, D. et al. (2021) Pollen Geochronology from the Atlantic Coast of the United States during the Last 500 Years. *Water*, 13, 362.
- Dangendorf, S., Hay, C., Calafat, F.M., Marcos, M., Piecuch, C.G., Berk, K. et al. (2019) Persistent acceleration in global sea-level rise since the 1960s. *Nature Climate Change*, 9(9), 705–710.
- Das, O., Wang, Y., Donoghue, J., Xu, X., Coor, J., Elsner, J. et al. (2013) Reconstruction of paleostorms and paleoenvironment using geochemical proxies archived in the sediments of two coastal lakes in northwest Florida. *Quaternary Science Reviews*, 68, 142–153.
- Dean, W.E. (1974) Determination of carbonate and organic matter in calcareous sediments and sedimentary rocks by loss on ignition: Comparison with other methods. *Journal of Sedimentary Petrology*, 44(1), 242–248.
- Donato, S.V., Reinhardt, E.G., Boyce, J.I., Pilarczyk, J.E. & Jupp, B.P. (2009) Particle-size distribution of inferred tsunami deposits in Sur Lagoon, Sultanate of Oman. *Marine Geology*, 257, 54–64.
- Donnelly, J.P., Butler, J., Roll, S., Wengren, M. & Webb, T. (2004) A backbarrier overwash record of intense storms from Brigantine, New Jersey. *Marine Geology*, 210, 107–121.
- Donnelly, J.P., Hawkes, A.D., Lane, P., MacDonald, D., Shuman, B.N., Toomey, M.R. et al. (2015) Climate forcing of unprecedented intense-hurricane activity in the last 2000 years. *Earth's Future*, 3, 49–65.
- Donnelly, J.P., Roll, S., Wengren, M., Butler, J., Lederer, R. & Webb, III T. (2001a) Sedimentary evidence of intense hurricane strikes from New Jersey. *Geology*, 29(7), 615–618.

14

Hausmann, N. et al. (2001b) 700 yr sedimentary record of intense hurricane landfalls in southern New England. *Geological Society of America Bulletin*, 113(6), 714–727.

- Donnelly, J.P. & Webb, T. (2004) Back-barrier Sedimentary Records of Intense Hurricane Landfalls in the Northeastern United States. In: Murane, R.J. & Liu, K., (Eds.) *Hurricanes and Typhoons: Past, Present, and Future.* Columbia University Press. pp. 58–95.
- Folk, R.L. & Ward, W.C. (1957) Brazos River bar [Texas]; a study in the significance of grain size parameters. *Journal of Sedimentary Research*, 27(1), 3–26.
- Gobeil, C., Tessier, A. & Couture, R.-M. (2013) Upper Mississippi Pb as a mid-1800s chronostratigraphic marker in sediments from seasonally anoxic lakes in Eastern Canada. *Geochimica et Cosmochimica Acta*, 113, 125–135.
- Graney, J.R., Halliday, A.N., Keeler, G.J., Nriagu, J.O., Robbins, J.A. & Norton, S.A. (1995) Isotopic record of lead pollution in lake sediments from the northeastern United States. *Geochimica et Cosmochimica Acta*, 59(9), 1715–1728.
- Haslett, J. & Parnell, A. (2008) A simple monotone process with application to radiocarbon-dated depth chronologies. *Applied Statistics*, 57(4), 399–418.
- Hawkes, A.D. & Horton, B.P. (2012) Sedimentary record of storm deposits from Hurricane Ike, Galveston and San Luis Islands, Texas. *Geomorphology*, 171–172, 180–189.
- Hippensteel, S.P. (2011) Spatio-lateral continuity of hurricane deposits in back-barrier marshes. *Geological Society of America Bulletin*, 123(11/12), 2277–2294.
- Hippensteel, S.P. & Garcia, W.J. (2014) Micropaleontological Evidence of Prehistoric Hurricane Strikes from Southeastern North Carolina. *Journal of Coastal Research*, 298(6), 1157–1172.
- Hippensteel, S.P. & Martin, R.E. (1999) Foraminifera as an indicator of overwash deposits, Barrier Island sediment supply, and Barrier Island evolution: Folly Island, South Carolina. *Palaeogeography, Palaeoclimatology, Palaeoecology*, 149, 115–125.
- Hong, I., Pilarczyk, J.E., Horton, B.P., Fritz, H.M., Kosciuch, T.J., Wallace, D.J. et al. (2018) Sedimentological characteristics of the 2015 Tropical Cyclone Pam overwash sediments from Vanuatu, South Pacific. *Marine Geology*, 396, 205–214.
- Horton, B.P. & Edwards, R.J. (2006) Quantifying Holocene Sea Level Change Using Intertidal Foraminifera: Lessons from the British Isles. Cushman Foundation Special Publication, 40, 1–97.
- Horton, B.P., Rossi, V. & Hawkes, A.D. (2009) The sedimentary record of the 2005 hurricane season from the Mississippi and Alabama coastlines. *Quaternary International*, 195, 15–30.
- Horton, B.P. & Sawai, Y. (2010) Diatoms as indicators of former sea levels, earthquakes, tsunamis, and hurricanes. *The Diatoms: Applications for the Environmental and Earth Sciences*, 2, 375–372.
- Johnson, C.S., Miller, K.G., Browning, J.V., Kopp, R.E., Khan, N.S., Fan, Y. et al. (2018) The role of sediment compaction and groundwater withdrawal in local sea-level rise, Sandy Hook, New Jersey, USA. *Quaternary Science Reviews*, 181, 30–42.
- Joyse, K.M., Khan, N.S., Moyer, R.P. et al. (2023). The preservation of Hurricane Irma's overwash deposit in southern Florida, USA. Marine Geology, 461, 107077.
- Kemp, A.C., Horton, B.P., Vane, C.H., Bernhardt, C.E., Corbett, D.R., Engelhart, S.E. et al. (2013) Sea-level change during the last 2500 years in New Jersey, USA. *Quaternary Science Reviews*, 81, 90–104.
- Kemp, A.C., Sommerfield, C.K., Vane, C.H., Horton, B.P., Chenery, S., Anisfeld, S. et al. (2012) Use of lead isotopes for developing chronologies in recent salt-marsh sediments. *Quaternary Geochro*nology, 12, 40–49.
- Khan, N.S., Vane, C.H., Horton, B.P. et al. (2015b) The application of δ^{13} C, TOC and C/N geochemistry to reconstruct Holocene relative sea levels and paleoenvironments in the Thames Estuary, UK. *Journal of Quaternary Science*, 30(5), 417–433.
- Khan, N.S., Vane, C.H. & Horton, B.P. (2015a) Stable carbon isotope and C/N geochemistry of coastal wetland sediments as a sea-level indicator. In: Shennan, I., Long, A.J. & Horton, B.P., (Eds.) *Handbook of Sea-Level Research*, First Edition. John Wiley & Sons, Ltd. pp. 295–311.
- Kiage, L.M., Deocampo, D., McCloskey, T.A., Bianchette, T.A. & Hursey, M. (2011) A 1900-year paleohurricane record from Wassaw

- Island, Georgia, USA. *Journal of Quaternary Science*, 26(7), 714–722.
- Kopp, R.E., Andrews, C., Broccoli, A., Garner, A., Kreeger, D., Leichenko, R. et al. (2019). New Jersey's Rising Seas and Changing Coastal Storms: Report of the 2019 Science and Technical Advisory Panel. Rutgers, The State University of New Jersey. Prepared for the New Jersey Department of Environmental Protection. Trenton, New Jersey.
- Lambert, W.J., Aharon, P. & Rodriguez, A.B. (2008) Catastrophic hurricane history revealed by organic geochemical proxies in coastal lake sediments: A case study of Lake Shelby, Alabama (USA). *Journal of Paleolimnology*, 39, 117–131.
- Lima, A.L., Bergquist, B.A., Boyle, E.A., Reuer, M.K., Dudas, F.O., Reddy, C.M. et al. (2005) High-resolution historical records from Pettaquamscutt River basin sediments: 2. Pb isotopes reveal a potential new stratigraphic marker. *Geochimica et Cosmochimica Acta*, 69(7), 1813–1824.
- Lin, N., Lane, P., Emanuel, K.A., Sullivan, R.M. & Donnelly, J.P. (2014) Heightened hurricane surge risk in northwest Florida revealed from climatological-hydrodynamic modeling and paleorecord reconstruction. *Journal of Geophysical Research: Atmospheres*, 119, 8606–8623.
- Liu, K. & Fearn, M.L. (1993) Lake-sediment record of late Holocene hurricane activities from coastal Alabama. *Geology*, 21, 793–796.
- Liu, K. & Fearn, M.L. (2000) Reconstruction of Prehistoric Landfall Frequencies of Catastrophic Hurricanes in Northwestern Florida from Lake Sediment Records. *Quaternary Research*, 54, 238–245.
- Liu, K. (2004) Paleotempestology: Principles, Methods, and Examples from Gulf Coast Lake Sediments. In: Murane, R.J. & Liu, K., (Eds.) *Hurricanes and Typhoons: Past, Present, and Future*. Columbia University Press. pp. 13–57.
- Ludlum, D.M. (1963) *Early American Hurricanes, 1492-1870*. American Meteorological Society.
- Maio, C.V., Donnelly, J.P., Sullivan, R., Madsen, S.M., Weidman, C.R., Gontz, A.M. et al. (2016) Sediment dynamics and hydrographic conditions during storm passage, Waquoit Bay, Massachusetts. *Marine Geology*, 381, 67–86.
- Mendelsohn, R., Emanuel, K., Chonabayashi, S. & Bakkensen, L. (2012) The impact of climate change on global tropical cyclone damage. *Nature Climate Change*, 2(3), 205–209.
- Muller, J., Collins, J.M., Gibson, S. et al. (2017) Recent Advances in the Emerging Field of Paleotempestology. In: Collins, J.M., Walsh, K., (Eds.) *Hurricanes and Climate Change*, 3. Springer. pp. 1–33.
- NOAA (2021). NOAA Tides and Currents. https://tidesandcurrents.noaa.gov/.
- NOAA (2022). *Historical Hurricane Tracks*. https://coast.noaa.gov/hurricanes/#map=4/32/-80.
- Pilarczyk, J.E., Dura, T., Horton, B.P., Engelhart, S.E., Kemp, A.C. & Sawai, Y. (2014) Microfossils from coastal environments as indicators of paleo-earthquakes, tsunamis and storms. *Palaeogeo-graphy, Palaeoclimatology, Palaeoecology*, 413, 144–157.
- Pilarczyk, J.E., Horton, B.P., Soria, J.L.A., Switzer, A.D., Siringan, F., Fritz, H.M. et al. (2016) Micropaleontology of the 2013 Typhoon Haiyan overwash sediments from the Leyte Gulf, Philippines. *Sedimentary Geology*, 339, 104–114.
- Pilarczyk, J.E., Horton, B.P., Witter, R.C., Vane, C.H., Chagué-Goff, C. & Goff, J. (2012) Sedimentary and foraminiferal evidence of the 2011 Tōhoku-oki tsunami on the Sendai coastal plain, Japan. *Sedimentary Geology*, 282, 78–89.
- Ranson, M., Kousky, C., Ruth, M., Jantarasami, L., Crimmins, A. & Tarquinio, L. (2014) Tropical and extratropical cyclone damages under climate change. *Climatic Change*, 127(2), 227–241.
- Rappaport, E.N. (2014) Fatalities in the United States from Atlantic Tropical Cyclones: New Data and Interpretation. *Bulletin of the American Meteorological Society*, 95(3), 341–346.
- Reimer, P.J., Austin, W.E.N., Bard, E., Bayliss, A., Blackwell, P.G., Bronk Ramsey, C. et al. (2020) The INTCAL20 Northern Hemisphere Radiocarbon Age Calibration Curve (0-55 CAL kBP). *Radiocarbon*, 62(4), 725–757.
- Ritchie, J.C. & McHenry, J.R. (1990) Application of Radioactive Fallout Cesium-137 for Measuring Soil Erosion and Sediment Accumulation

1. Downloaded from https://onlinelibrary.viley.com/doi/10.1002/jqs.3622 by Rutgers University Libraries, Wiley Online Library on [29/05/2024]. See the Terms and Conditions (https://onlinelibrary.viley.com/terms-ad-conditions) on Wiley Online Library for rules of use; OA articles are governed by the applicable Creative Commons Licenses

- Rates and Patterns: A Review. *Journal of Environmental Quality*, 19, 215–233.
- Scileppi, E. & Donnelly, J.P. (2007) Sedimentary evidence of hurricane strikes in western Long Island, New York. Geochemistry, Geophysics, Geosystems, 8(6), 1–25.
- La Selle, S.M., Lunghino, B.D., Jaffe, B.E., Gelfenbaum, G. & Costa, P.J.M. (2017) Hurricane Sandy Washover Deposits on Fire Island, New York (Open File Report No. 2017–2014; p. 30). United States Geological Survey.
- Seneviratne, S.I., Zhang, X., Adnan, M. et al. (2021) Climate Change 2021: The Physical Science Basis. Contribution of Working Group I to the Sixth Assessment Report of the Intergovernmental Panel on Climate Change.
- Shaw, J. & Ceman, J. (1999) Salt-marsh aggradation in response to late-Holocene sea-level rise at Amherst Point, Nova Scotia, Canada. *The Holocene*, 9(4), 439–451.
- Simbo, C.W., Potra, A. & Samuelsen, J.R. (2019) A geochemical evaluation of the genetic relationship between Ouachita Mountains Paleozoic rocks and the Mississippi Valley-type mineralization in the southern Ozark Region, USA. Ore Geology Reviews, 112, 103029.
- Soria, J.L.A., Switzer, A.D., Pilarczyk, J.E., Siringan, F.P., Khan, N.S. & Fritz, H.M. (2017) Typhoon Haiyan overwash sediments from Leyte Gulf coastlines show local spatial variations with hybrid storm and tsunami signatures. Sedimentary Geology, 358, 121–138.
- Sweet, W.V., Hamlington, B.D., Kopp, R.E., Weaver, C.P., Barnard, P.L., Bekaert, D. et al., (2022) Global and Regional Sea Level Rise Scenarios for the United States: Updated Mean Projections and Extreme Water Level Probabilities Along U.S. Coastlines. NOAA Technical Report NOS 01. National Oceanic and Atmospheric Administration, National Ocean Service, Silver Spring, MD, pp. 111 https://oceanservice.noaa. gov/hazards/sealevelrise/noaa-nostechrpt01-global-regional-SLRscenarios-US.pdf
- Talke, S.A., Orton, P. & Jay, D.A. (2014) Increasing storm tides in New York Harbor, 1844-2013. Geophysical Research Letters, 41, 3149–3155.
- Troels-Smith, J. (1955) Characterization of unconsolidated sediments (Vol. 3). Reitzels Forlag.
- U.S. Geological Survey. (1943) USGS 1:25000-scale Quadrangle for South Amboy, NJ 1943 [Map]. U.S. Geological Survey.
- U.S. Geological Survey. (1954) USGS 1:24000-scale Quadrangle for South Amboy, NJ 1954 [Map]. U.S. Geological Survey.
- Vane, C.H., Jones, D.G. & Lister, T.R. (2009) Mercury contamination in surface sediments and sediment cores of the Mersey Estuary, UK. *Marine Pollution Bulletin*, 58, 940–946.
- Walker, J.S., Cahill, N., Khan, N.S., Shaw, T.A., Barber, D., Miller, K.G. et al. (2020) Incorporating temporal and spatial variability of salt-marsh foraminifera into sea-level reconstructions. *Marine Geology*, 429, 106293.
- Walker, J.S., Kopp, R.E., Little, C.M. & Horton, B.P. (2022) Timing of emergence of modern rates of sea-level rise by 1863. *Nature Communications*, 13, 966.
- Walker, J.S., Kopp, R.E., Shaw, T.A., Cahill, N., Khan, N.S., Barber, D.C. et al. (2021) Common Era sea-level budgets along the U.S. Atlantic coast. *Nature Communications*, 12, 1841.
- Wallace, D.J., Woodruff, J.D., Anderson, J.B. & Donnelly, J.P. (2014) Palaeohurricane reconstructions from sedimentary archives along the Gulf of Mexico, Caribbean Sea and western North Atlantic Ocean margins. *Geological Society, London, Special Publications*, 388, 481–501.
- Wallace, E.J., Dee, S.G. & Emanuel, K.A. (2021) Resolving Long-Term Variations in North Atlantic Tropical Cyclone Activity Using a Pseudo Proxy Paleotempestology Network Approach. *Geophysical Research Letters*, 48, 1–13.
- Williams, H.F.L. (2009) Stratigraphy, Sedimentology, and Microfossil Content of Hurricane Rita Storm Surge Deposits in Southwest Louisiana. *Journal of Coastal Research*, 254(4), 1041–1051.
- Williams, H.F.L. (2010) Storm surge deposition by Hurricane Ike on the McFaddin National Wildlife Refuge, Texas: Implications for paleotempestology studies. *The Journal of Foraminiferal Research*, 40(3), 210–219.

Appendix 1

Chronology methodology

Levels of ¹³⁷Cs in CQM-3 were measured in bulk (1-cm-thick) samples every 2 cm via gamma spectroscopy at East Carolina University. The initial increase in ¹³⁷Cs activity indicates when fallout from the beginning of nuclear weapons testing became detectable in salt marsh sediments in 1954 cE (Ritchie & McHenry, 1990). The subsequent spike in ¹³⁷Cs activity shows where levels of nuclear weapons testing peaked in 1963 cE and thereafter began to fall as a result of the 1963 Test Ban Treaty (Ritchie & McHenry, 1990).

Concentrations of Pb are assumed to reflect changes in the production, consumption and subsequent emission of Pb in the USA throughout the 19th and 20th centuries (Graney et al., 1995, Kemp et al., 2012). Samples were analyzed by ICP-MS at the Meadowlands Research & Restoration Institute. Given the tendency for heavy metal pollutants to be closely associated with organic content in cores (Vane et al., 2009, Kemp et al., 2013), bulk Pb concentrations were normalized to organic matter measured via LOI in CQM-3. The chronohorizon in bulk Pb was assigned to a depth corresponding with peak Pb concentrations in CQM-3 following Lima et al. (2005), Kemp et al. (2012, 2013), Gobeil et al. (2013) and Walker et al. (2021).

Pb isotopic ratios (206Pb:207Pb) were measured in bulk (1cm-thick) samples every 4 cm from CQM-3 at University of Georgia's Center for Applied Isotope Studies to provide additional historical chronohorizons to constrain the timing of sedimentation within the core. Samples were prepared by heating sediments at 375 °C for 5 h to burn off any organic carbon. Approximately 50 mg of crushed and homogenized sediment from each sample was treated with an HNO₃-HCl acid attack to solubilize any anthropogenic Pb from the sediments (Graney et al., 1995). The Pbcontaining leachate was separated and prepared for stable Pb isotope analysis following the procedures of Simbo et al. (2019). Stable Pb isotope measurements were completed using an ICP-MS (Nu Plasma II). Stable Pb isotope chronohorizons were assigned to depths in CQM-3 following Lima et al. (2005), Kemp et al. (2012, 2013) and Gobeil et al. (2013).

Palynomorphs (pollen grains and fern spores) were extracted from 1-cm-thick sediment samples collected every 4 cm from CQM-3 and prepared for counting at the University of Minnesota's Continental Scientific Drilling Facility following the procedure of Bennet and Willis (2002). A total of 300 pollen grains were counted from each sample to find the relative abundance of *Ambrosia* and *Quercus* pollen. Three pollen chronohorizons were assigned to depths in CQM-3 following Christie et al. (2021).

Radiocarbon ages were produced from organic material sampled below 100 cm within CQM-3 to constrain the age of the oldest overwash deposit within the core. *In situ* woody plant materials were extracted from sediments within the core and were cleaned of any contaminating sediments or younger roots under a microscope (e.g. Kemp et al. 2013). Cleaned samples were dried overnight at 45 °C and measured for dry weight (Kemp et al. 2013). Samples were submitted to Beta Analytic, where samples underwent an acid–base–acid pretreatment before being analyzed via accelerator mass spectrometry. Reported radiocarbon ages and their uncertainties (Table 2) were calibrated using the INTCAL20 dataset (Reimer et al., 2020).